

SPIN CORRELATIONS IN MnO

I. A. BLECH and B. L. AVERBACH

Department of Metallurgy, Massachusetts Institute of Technology

(Received 30 March 1964; in revised form 13 May 1964)

Abstract

Spin correlations have been investigated in powder samples of MnO above and below the Néel temperature by means of diffuse neutron scattering measurements. There is a significant local order above T_N , with the spins coupled in an antiferromagnetic fashion and tending to lie parallel to $\{111\}$ planes. This layer structure suggests a second neighbor interaction energy, with $V_2 = 4.9 \times 10^{-3}$ eV and with the exchange interaction $J_2 = -4.6^\circ$. There was no evidence for an extra total scattering in the vicinity of the critical temperature.

I. Introduction

MANGANOUS oxide is antiferromagnetic [1] with a Néel temperature of about 120°K . The chemical cell has the NaCl structure, and the magnetic cell is twice as big with a parameter of 8.85 \AA [2]. The net spins of the manganese ions are parallel to $\{111\}$ planes, with the spins on a given $\{111\}$ plane in the same direction and thus ferromagnetically coupled [3]. Spins on adjacent $\{111\}$ planes are oppositely directed and the antiferromagnetic coupling is indirect through oxygen atoms by a superexchange mechanism. The ordered antiferromagnetic structure thus consists of layers of alternately directed spins, all parallel to $\{111\}$ planes; below the Néel temperature, the structure is rhombohedral with a cell parameter of 8.873 \AA and a rhombohedral angle of $90^\circ 26'$ at 4.2°K . The direction of the spins within the $\{111\}$ plane has not been determined experimentally, but it has been suggested [4] that the spins are in $\{1\bar{1}0\}$ directions.

The spin arrangement above the critical temperature had not been determined in MnO. An investigation of CoO by means of neutron diffraction [5] indicated that there was some spin correlation above the Néel temperature, and that the correlation range was quite large. We have investigated the local spin correlation above and below the Néel temperature in polycrystalline MnO by observations of the diffuse neutron scattering of thermal neutrons. It was necessary to define a correlation coefficient γ_i , which is related to the probability that a spin in the i 'th shell of manganese ions about a given manganese ion is parallel to the spin at the origin, and another coefficient Γ_i which is related to the probability that the spins are parallel to a given direction. The latter directional correlation has not been clearly recognized before, and scattering equations necessary to show this are developed in Section III. We have assumed, along with others, that there is no energy transfer between the entering neutron beam and the spin system in the sample. This quasistatic approximation may not be strictly correct, but it probably does not greatly affect the main conclusions.

Finally, in the last section, we consider the question of the critical scattering of neutrons as the sample is taken through the Néel temperature. There is some confusion in the definition of critical scattering, but we show that there is no unusual increase in the total scattering cross section of MnO near the critical.

II. Experimental Procedure

MnO powder was obtained by reducing MnCO_3 at 1000°C for two hours under dry hydrogen. The resultant MnO was checked by X-ray diffraction and chemical analysis and was packed into aluminum

cylindrical sample holders under a dry helium atmosphere. A liquid nitrogen vacuum cryostat mounted on the neutron diffraction spectrometer was used to cool the sample to about 80°K and the temperature of the specimen was controlled within $\pm 1^\circ\text{C}$ at intermediate temperatures by means of a small heater. The apparent temperature of the sample in the cryostat was consistently high by about 3°C , judging from the comparison of our measured Néel temperature with the accepted value.

The diffraction experiments were carried out at the MIT nuclear reactor. Unpolarized thermal neutrons were monochromated by diffraction from the $\{111\}$ planes of a lead crystal in transmission to give an average wavelength of 1.20 \AA . A Soller slit system was used to collimate the diffracted beam into a heavily shielded BF_3 detector, and the diffraction angle was determined within one minute of arc. Runs were also made with an empty sample holder and with a dummy cadmium holder in order to obtain the usual parasitic and background scattering corrections.

A typical series of measurements for samples below the Néel temperature are shown in Figure 1. There is a strong $\{111\}$ coherent peak in the vicinity of 14 degrees in 2θ which arises from the ordered antiferromagnetic structure. It should be noted, however, that the sharp peak sits atop a broad diffuse hump which grows progressively more pronounced as the temperature is raised. This diffuse peak indicates that the spin

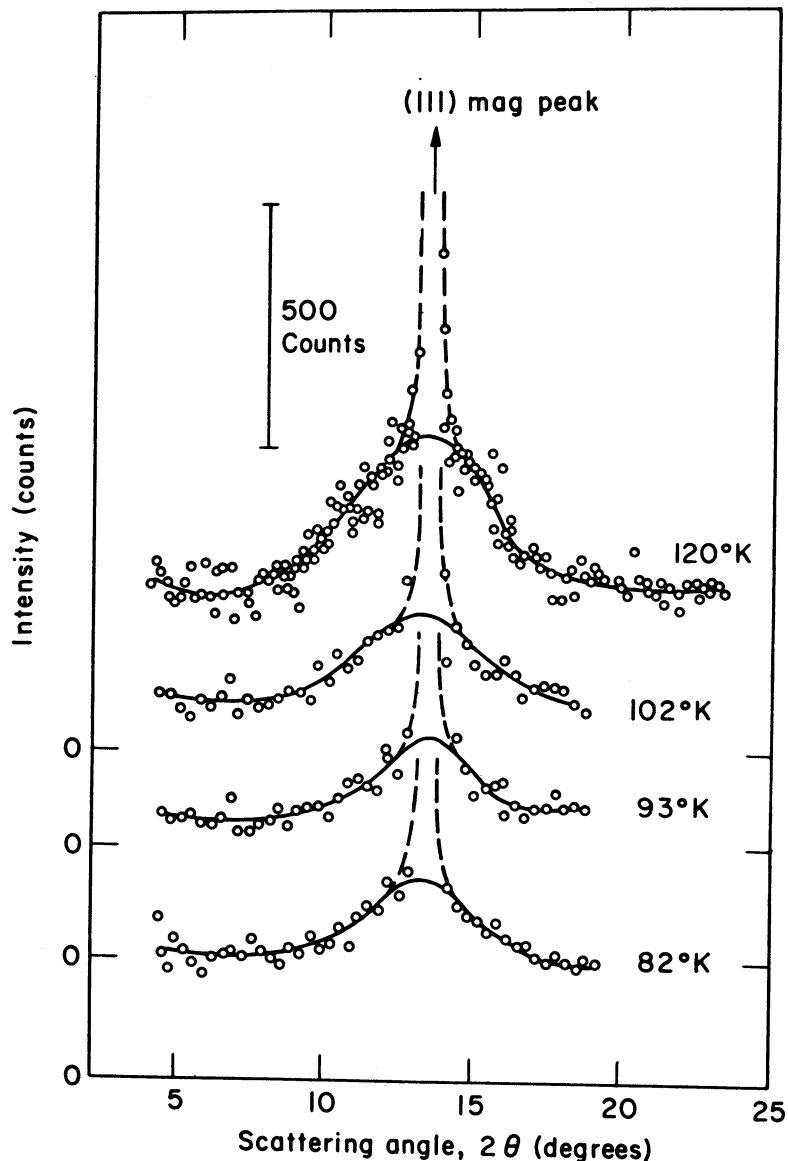


FIGURE 1
Intensity in vicinity of (111) magnetic peak below the Néel temperature.

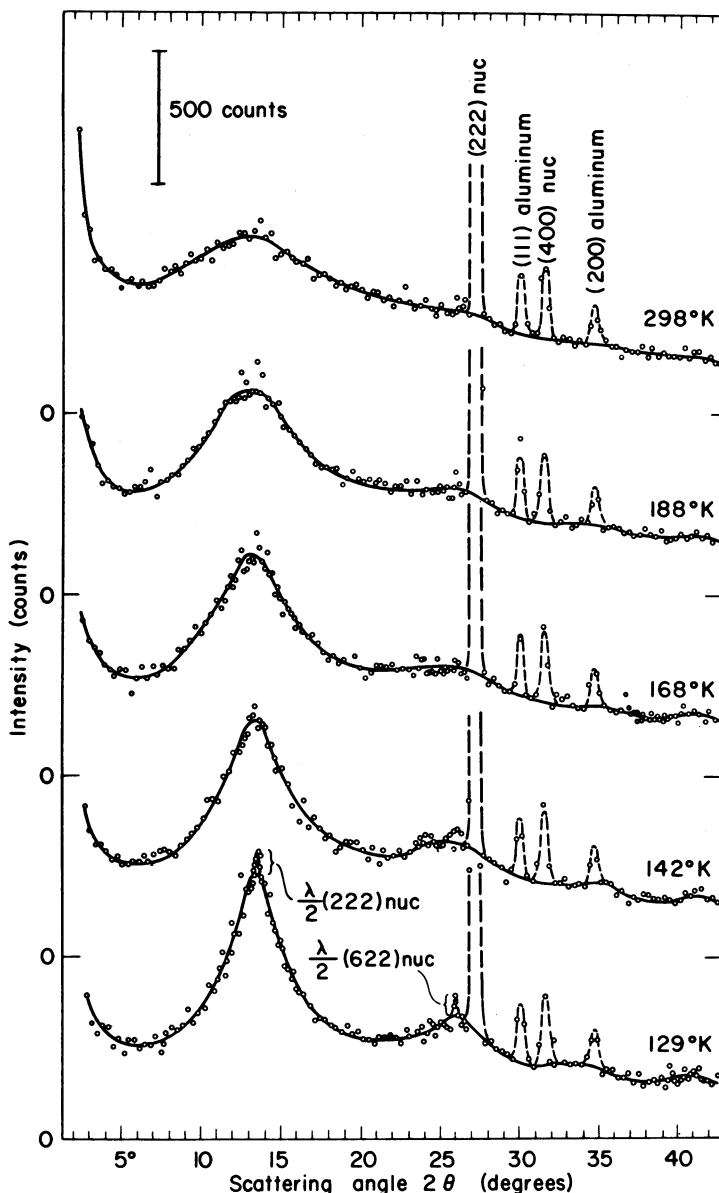


FIGURE 2
Diffuse scattering above the Néel temperature.

order is not perfect and that some disorder exists within the ordered antiferromagnetic structure. Figure 2 shows the data for samples above the Néel temperature. A very small sharp peak persists, and this is the half-wavelength from the $\{222\}$ nuclear peak. The half-wavelength intensity is very small, however, and this contribution was eliminated by inspection. A strong diffuse peak remains in the vicinity of the $\{111\}$ magnetic peak position, and this was clearly evident at temperatures up to room temperature.

The scattered intensity was converted into absolute units by comparison with the known incoherent scattering from vanadium. This involved a correction for the multiple diffuse scattering of an incoherent scatterer which will be described elsewhere. The standardization was also obtained by comparison with the $\{111\}$ peak from nickel and the $\{622\}$ peak from MnO. These standardization procedures all yielded consistent results.

The diffuse scattering was corrected for three additional contributions. The nuclear spin incoherent scattering was evaluated, using incoherent cross sections listed by Bacon [6]. The temperature diffuse scattering was estimated by means of the usual Debye approximation using an average Debye temperature of 502°K [7]. One of the principal corrections arose from the multiple scattering in MnO. This scattering arises from multiple Bragg scattering events which diffract extra intensity into the horizontal plane. An ap-

proximate calculation was made, but the correction was made experimentally in the following way. A series of diffuse intensity measurements were made with MnO powder in a cylindrical sample holder in which thin cadmium discs were spaced evenly along the sample. Four different disc spacings were used and the diffuse scattering per unit volume of MnO decreased systematically as the disc spacing was decreased. An extrapolation to zero disc spacing provided the correction for the multiple scattering. Several attenuation experiments were also performed in order to obtain an absorption correction for the cylindrical sample. The net diffuse scattering was analyzed by means of a Fourier transform. The transform has the advantage that slowly varying errors in the various corrections contribute spurious detail at the very beginning of the transform function, and it was possible to separate these effects from the significant portions of the transforms at distances corresponding to atomic positions.

The net diffuse paramagnetic scattering is shown on an absolute basis in Figures 3 and 4. At temperatures below the critical, Figure 3, the diffuse intensity is well below the curve for random paramagnetic

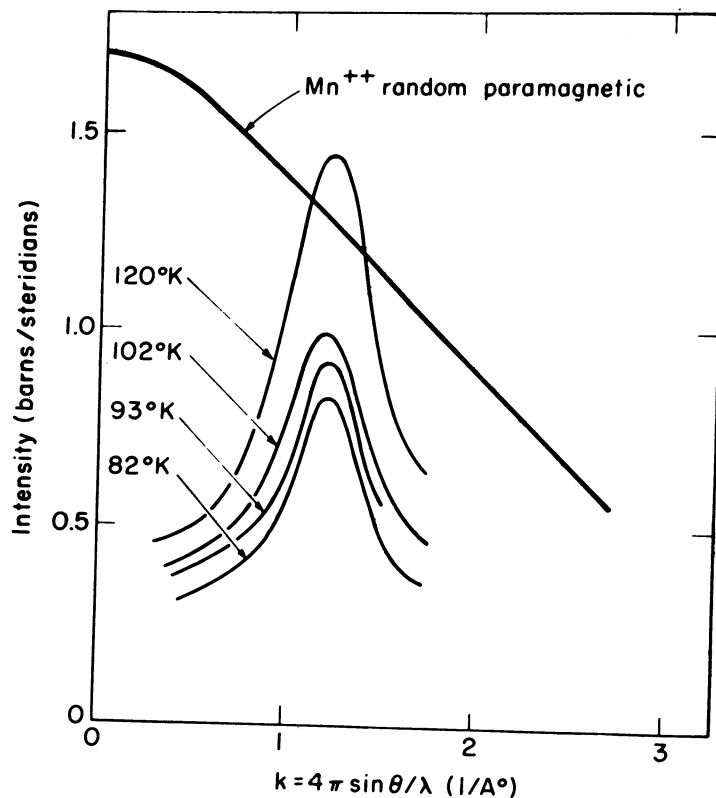


FIGURE 3
Net diffuse paramagnetic scattering at temperatures below T_N .

scattering which is calculated for the case where all of the Mn^{++} ions in the crystal are scattering incoherently. A large fraction of the ions are scattering coherently into the $\{111\}$ magnetic peak in this region, and the diffuse scattering arises from the local disorder. Above the critical temperature, Figure 4, all of the Mn^{++} ions are scattering into the diffuse peaks and the paramagnetic scattering modulates the random curve, as expected. The presence of strong diffuse humps in Figure 4 indicates that the spin correlation is pronounced for temperatures well above the Néel temperature.

III. Analysis of the Data

We assume the quasistatic approximation for the diffuse magnetic scattering and start with the equation given by de Gennes [8] for the magnetic scattering of unpolarized neutrons.

$$\frac{d\sigma}{d\Omega} = \left(\frac{e^2\gamma}{mc^2}\right)^2 \sum_{mm'} f_m^* f_{m'} \langle \bar{S}_{m1} \cdot \bar{S}_{m'1} \rangle \exp [i \bar{k} \cdot (\bar{R}_m - \bar{R}_{m'})] \quad (1)$$

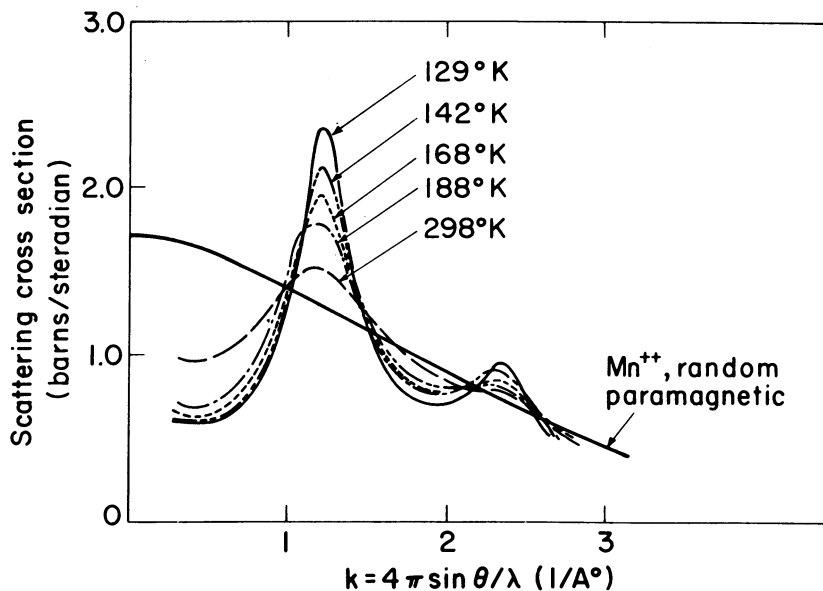


FIGURE 4
Net diffuse scattering at temperatures above T_N .

where $\frac{d\sigma}{d\Omega}$ is the differential scattering cross section, γ the magnetic moment of neutrons expressed in nuclear magnetons, e the electron charge, m the electron mass, and c the velocity of light. The quantities f_m and $f_{m'}$ are the magnetic amplitude form factors for atoms at sites m and m' respectively, and for MnO this becomes $f_m = f_{m'} = f$, where f is the Mn^{++} magnetic form factor. The quantities $\bar{S}_{m\perp}$ and $\bar{S}_{m'\perp}$ are the projections of the spin vectors at m and m' on the diffraction plane, as shown in Figure 5a. The quantity $\bar{k} = \frac{2\pi}{\lambda}(\bar{s} - \bar{s}_0)$ is the diffraction vector, where \bar{s}_0 and \bar{s} are unit vectors parallel to the incident and to the diffracted beams respectively. \bar{R}_m and $\bar{R}_{m'}$ are vectors from an arbitrary origin to the sites m and m' respectively. It is evident from equation (1) that the "spin-only" magnetic scattering arises from the components of the spin which are normal to the diffraction plane, i.e., from the components lying in the diffraction plane.

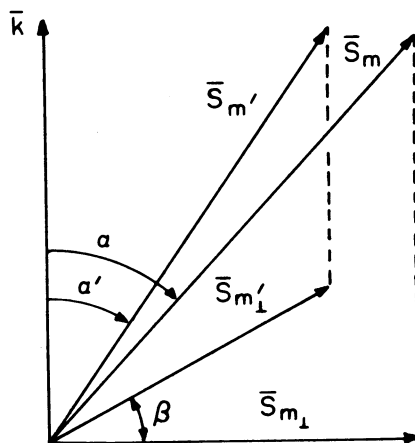


FIGURE 5a
Vectors $\bar{S}_{m\perp}$ and $\bar{S}_{m'\perp}$ are components of the spin vectors \bar{S}_m and $\bar{S}_{m'}$ which lie in the plane normal to the diffraction vector \bar{k} .

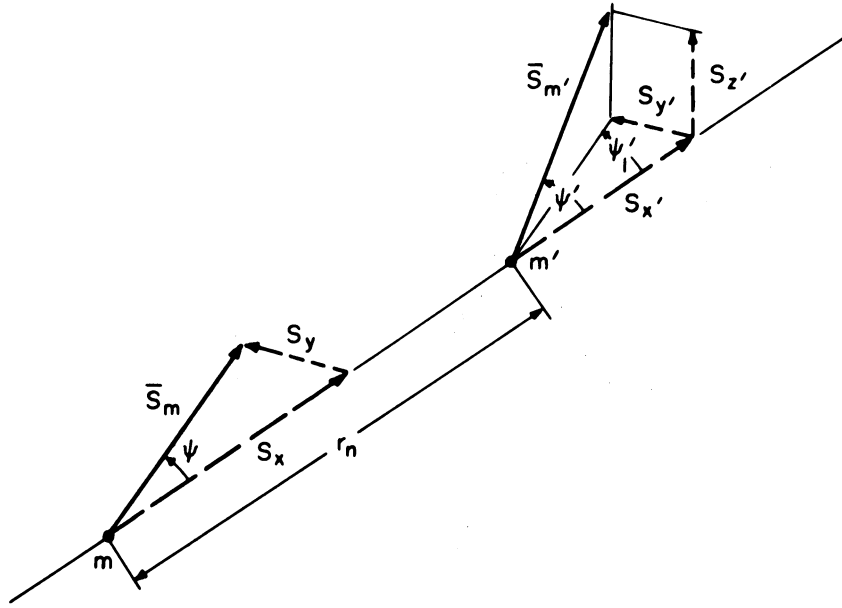


FIGURE 5b

Spin vectors \bar{S}_m and $\bar{S}_{m'}$ and their projections on the line r_n .

Using the geometric relations in Figure 5a, the scattering, $\frac{d\sigma}{d\Omega}$, from a particular spin pair m', m can be rewritten as,

$$\frac{d\sigma}{d\Omega} = \frac{1}{2} \left(\frac{e^2 \gamma}{mc^2} \right)^2 f^2 \sin a \sin a' \cos \beta |\bar{S}_m| |\bar{S}_{m'}| \{ \exp [-i \bar{k} \cdot (\bar{R}_m - \bar{R}_{m'})] + \exp [i \bar{k} \cdot (\bar{R}_m - \bar{R}_{m'})] \} \quad (2)$$

where the angles a, a' and β are defined in Figure 5a. The average scattering for all pairs separated by the distance r_n , where $\bar{r}_n = \bar{R}_m - \bar{R}_{m'}$ is

$$\frac{d\sigma}{d\Omega} = \left(\frac{e^2 \gamma}{mc^2} \right)^2 f^2 \langle |\bar{S}_m| |\bar{S}_{m'}| \sin a \sin a' \cos \beta \cos (k r_n \cos \phi) \rangle_n \quad (3)$$

there the bracket $\langle \rangle_n$ denotes the average over all pairs \bar{r}_n apart, and ϕ is the angle between \bar{r}_n and \bar{k} , as shown in Figure 6. Any spin pair m, m' can be resolved into the components shown in Figure 5b, and the scattering from such pairs may be written in terms of the contributions arising from all of the pairs of components. Thus,

$$\frac{d\sigma}{d\Omega} = \left(\frac{d\sigma}{d\Omega} \right)_{S_x S_{x'}} + \left(\frac{d\sigma}{d\Omega} \right)_{S_x S_{y'}} + \left(\frac{d\sigma}{d\Omega} \right)_{S_x S_{z'}} + \left(\frac{d\sigma}{d\Omega} \right)_{S_y S_{x'}} + \left(\frac{d\sigma}{d\Omega} \right)_{S_y S_{y'}} + \left(\frac{d\sigma}{d\Omega} \right)_{S_y S_{z'}} \quad (4)$$

Here a typical term, $\left(\frac{d\sigma}{d\Omega} \right)_{S_x S_{x'}}$, represents the scattering cross section due to the $S_x S_{x'}$ pair.

In a powder scattering experiment, a crystallite axis, \bar{r}_n , can take all relative orientations with respect to \bar{k} , and the crystallite can also be rotated about such an axis. The scattered intensity for any spin pair must be averaged accordingly, and we obtain

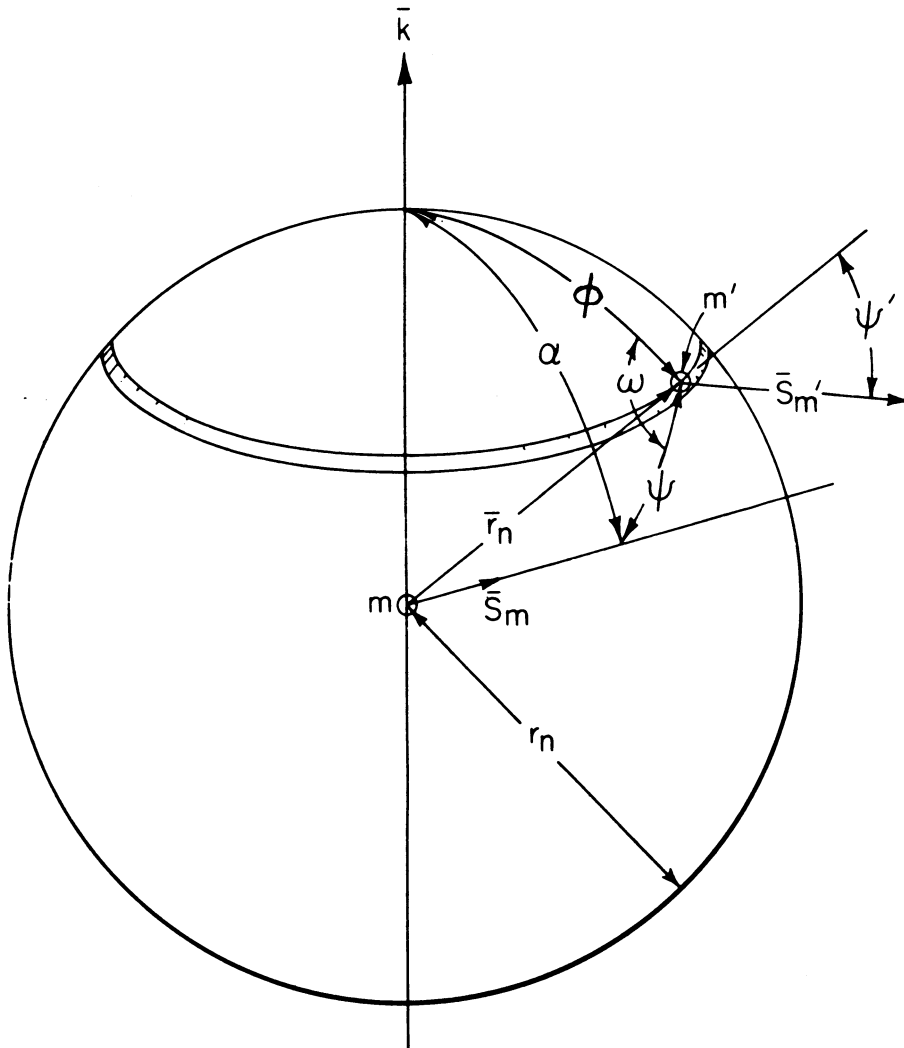
$$\begin{aligned} \frac{d\sigma}{d\Omega} &= \left(\frac{e^2 \gamma}{mc^2} \right)^2 f^2 \langle |\bar{S}_m| |\bar{S}_{m'}| \sin a \sin a' \cos \beta \cos (k r_n \cos \phi) \rangle_n \\ &= \frac{1}{4\pi r_n^2} \int_{\varphi=0}^{\pi} \int_{\omega=0}^{2\pi} \langle |\bar{S}_m| |\bar{S}_{m'}| \sin a \sin a' \cos \beta \cos (k r_n \cos \phi) \rangle_n r_n^2 \sin \phi d\phi d\omega \end{aligned} \quad (5)$$

where ω is defined in Figure 6. The average on the right hand side of equation (5) can be written as a sum of six terms indicated in equation (4). The orthogonal terms vanish, leaving the two collinear terms,

$$\begin{aligned} \frac{d\sigma}{d\Omega} &= \left(\frac{d\sigma}{d\Omega}\right)_{S_x S_{x'}} + \left(\frac{d\sigma}{d\Omega}\right)_{S_y S_{y'}} \\ &= \left(\frac{\gamma e^2}{mc^2}\right)^2 f^2 \times \frac{1}{4\pi} \int_{\phi=0}^{\pi} \int_{\omega=0}^{2\pi} \{ \langle \bar{S}_x \cdot \bar{S}_{x'} \rangle_n \sin^2 \psi \\ &\quad + \langle \bar{S}_y \cdot \bar{S}_{y'} \rangle_n (1 - \sin^2 \psi \cos^2 \omega) \} \cos(kr_n \cos \phi) \sin \phi \, d\phi \, d\omega \end{aligned} \quad (6)$$

Integrating equation (6) leads to

$$\frac{d\sigma}{d\Omega} = \left(\frac{\gamma e^2}{mc^2}\right)^2 f^2 \left\{ a_n \frac{\sin kr_n}{kr_n} + b_n \left(\frac{\sin kr_n}{k^3 r_n^3} - \frac{\cos kr_n}{k^2 r_n^2} \right) \right\} \quad (7)$$



$\bar{k} = \frac{2\pi}{\lambda} (\bar{s} - \bar{s}_0)$ = unit vector parallel to diffraction vector
 $\bar{S}_m, \bar{S}_{m'}$ = spin vectors

FIGURE 6
 Geometrical diffraction relations.

where

$$\begin{aligned} a_n &= \langle \bar{S}_y \cdot \bar{S}_{y'} \rangle_n \\ b_n &= 2 \langle \bar{S}_x \cdot \bar{S}_{x'} \rangle_n - \langle \bar{S}_y \cdot S_{y'} \rangle_n \end{aligned} \quad (8)$$

Equations (8) can be written as follows:

$$\begin{aligned} a_n &= \langle (\bar{S}_m \cdot \bar{S}_{m'}) \frac{\sin \psi \sin \psi_1'}{\cos(\psi - \psi_1')} \rangle_n \\ b_n &= \langle (\bar{S}_m \cdot \bar{S}_{m'}) \left(\frac{2 \cos \psi \cos \psi_1' - \sin \psi \sin \psi_1'}{\cos(\psi - \psi_1')} \right) \rangle_n \end{aligned} \quad (9)$$

where ψ , ψ_1 , ψ_1' are defined in Figure 5.

The total differential cross section is accordingly,

$$\frac{d\sigma}{d\Omega} = \frac{2}{3} S(S+1) \left(\frac{\gamma e^2}{mc^2} \right)^2 f^2 + \left(\frac{e^2 \gamma}{mc^2} \right)^2 f^2 \sum_n \left\{ a_n \frac{\sin kr_n}{kr_n} + b_n \left(\frac{\sin kr_n}{k^3 r_n^3} - \frac{\cos kr_n}{k^2 r_n^2} \right) \right\} \quad (10)$$

where S is the spin quantum number. The first term on the right hand side represents the ideal paramagnetic scattering, i.e., the scattering from a random assembly of spins; the rest of the terms arise from spin pair correlations. The coefficients a_n and b_n are related to the probability of finding spin pairs with parallel components.

We now consider an atom at an arbitrary origin; this atom has c_i neighbors at a distance, r_i , from the origin, with the subscript i indicating the atom shell number. Allowing each atom in turn to be the origin, we may describe the modulations in the diffuse scattering in terms of a relative intensity, $I(k)$, where

$$\begin{aligned} I(k) &= \frac{d\sigma/d\Omega}{\frac{2}{3} S(S+1) \left(\frac{\gamma e^2}{mc^2} \right)^2 f^2} - 1 \\ &= \frac{3}{2} \sum_i c_i \left\{ \frac{a_i}{S(S+1)} \frac{\sin kr_i}{kr_i} + \frac{b_i}{S(S+1)} \left[\frac{\sin kr_i}{k^3 r_i^3} - \frac{\cos kr_i}{k^2 r_i^2} \right] \right\} \end{aligned} \quad (11)$$

The coefficients a_i and b_i are now averaged over all of the pairs in i^{th} shell. The coefficients a_n and b_n may be simplified if the spin at m' has a rotational symmetry about the direction of the spin at the origin. With this simplification the following definitions are convenient,

$$\frac{a_n}{S(S+1)} = \gamma_n A_n \quad (12)$$

$$\frac{b_n}{S(S+1)} = \gamma_n B_n$$

$$\gamma_n = \frac{\langle \bar{S}_m \cdot \bar{S}_{m'} \rangle}{S(S+1)}$$

$$A_n = \sin^2 \psi \quad (13)$$

$$B_n = 2 \cos^2 \psi - \sin^2 \psi$$

Equation (11) now becomes

$$I(k) = \frac{3}{2} \sum_{i=1} c_i \left\{ (\overline{\gamma A})_i \frac{\sin kr_i}{kr_i} + (\overline{\gamma B})_i \left(\frac{\sin kr_i}{k^3 r_i^3} - \frac{\cos kr_i}{k^2 r_i^2} \right) \right\} \quad (14)$$

where the quantities $(\overline{\gamma A})_i$ and $(\overline{\gamma B})_i$ are now averaged for each shell, i . Equation (14) is the quasistatic approximation for the modulation of the diffuse neutron scattering arising from the local order in the atomic magnetic moments. This equation is analogous to the expressions obtained for the diffuse scattering of X-rays by a binary system exhibiting short range order [9, 10]. In the X-ray case, however, the terms starting with $(\overline{\gamma B})$ do not appear; the latter terms arise from the directional nature of the magnetic neutron scattering.

The physical significance of the short range order coefficients γ_i , A_i and B_i may be examined in terms of the magnetic structure of the MnO. Below the Néel temperature, T_N , the structure involves layers of spins parallel to $\{111\}$ planes, with the layers coupled antiferromagnetically. The first shell of twelve nearest neighbor spins contains six parallel and six antiparallel spins, and the net moment for the first shell is thus zero. The second shell consists of six antiparallel spins. The third shell has a net zero moment; the fourth shell has 12 parallel spins, and so on as shown in Table 1. For convenience, we shall call the shells with mixed spins and a vanishing moment mixed shells, and the others, unmixed shells. However, even though $\overline{\gamma}_i = 0$ for a mixed shell, the products $(\overline{\gamma A})_i$ and $(\overline{\gamma B})_i$ may not vanish, since, in general, $(\overline{\gamma A})_i \neq \overline{\gamma}_i \overline{A}_i$ and $(\overline{\gamma B})_i \neq \overline{\gamma}_i \overline{B}_i$. There may thus be a diffuse scattering from the mixed shells even though the net moment is zero.

TABLE 1
Directional Factors x_i and y_i for $\{111\}$ and $\{100\}$ Models in Ordered MnO.

Shell number (i)	Mean spin alignment relative to origin	$\{111\}$ model		$\{100\}$ model	
		x_i	y_i	x_i	y_i
1	0	-0.25000	+0.75000	0	0
2	Antiparallel	-1	0	-1	0
3	0	0.08333	-0.25000	0	0
4	Parallel	+1	0	+1	0
5	0	0.15000	-0.45000	0	0
6	Antiparallel	-1	0	-1	0
7	0	-0.10710	0.32130	0	0
8	Parallel	+1	0	+1	0
9	0	-0.10190	+0.30570	0	0
10	Antiparallel	-1	0	-1	0

If there is no interrelationship between spin correlation and spin direction, then $(\overline{\gamma A})_i = \overline{\gamma}_i \overline{A}_i$ and $(\overline{\gamma B})_i = \overline{\gamma}_i \overline{B}_i$. The short range order coefficients vanish for the mixed shells. For the mixed shells $(\overline{\gamma A})_i = (2/3)\overline{\gamma}_i$ and $(\overline{\gamma B})_i = 0$. The resulting equation reduces to the X-ray case, and this reduced equation was used by McReynolds and Riste [5] in their analysis of the CoO diffuse scattering. In general, the larger the coefficients $(\overline{\gamma A})_i$ and $(\overline{\gamma B})_i$, the greater the local spin order. The quantity γ_i is positive for ferromagnetic coupling, and negative for antiferromagnetic coupling; A_i is always positive, but B_i may be negative. The terms in $(\overline{\gamma B})_i$ do not contribute as much to the scattering as the other terms since it decreases rapidly with kr , but the contribution is still significant.

It is difficult to separate the spin correlation coefficients γ_i from the directional functions A_i and B_i . Instead of attempting a best fit to the experimental transform in an analytical fashion we have assumed a few reasonable models of spin correlation, calculated the resulting transform, and compared with the experimental transform. The use of a digital computer greatly facilitated calculations of the experimental transforms and of the model transforms. Two models for the interdependence of spin correlation with spin direction were considered. In the $\{111\}$ model we assume that the spins in a given small region are parallel to a direction within the $\{111\}$ plane. In the $\{100\}$ model we assume that the spins in a local region are parallel to $\langle 100 \rangle$ directions.

We assume in each model that the absolute value of the individual spin correlation factor for a given shell i , γ_i , is constant. It is convenient to define quantities, $x_i = \frac{3}{2} \frac{(\gamma A)_i}{|\gamma_i|}$ and $y_i = \frac{3}{2} \frac{(\gamma B)_i}{|\gamma_i|}$. These quantities x_i and y_i are independent of the magnitude of the spin correlation. The coefficients x_i and y_i depend on the relative directions of the spins and are listed for the ordered MnO structure in Table 1 for the {111} and the {100} models. In the disordered condition, the spin correlations are disordered in two ways.

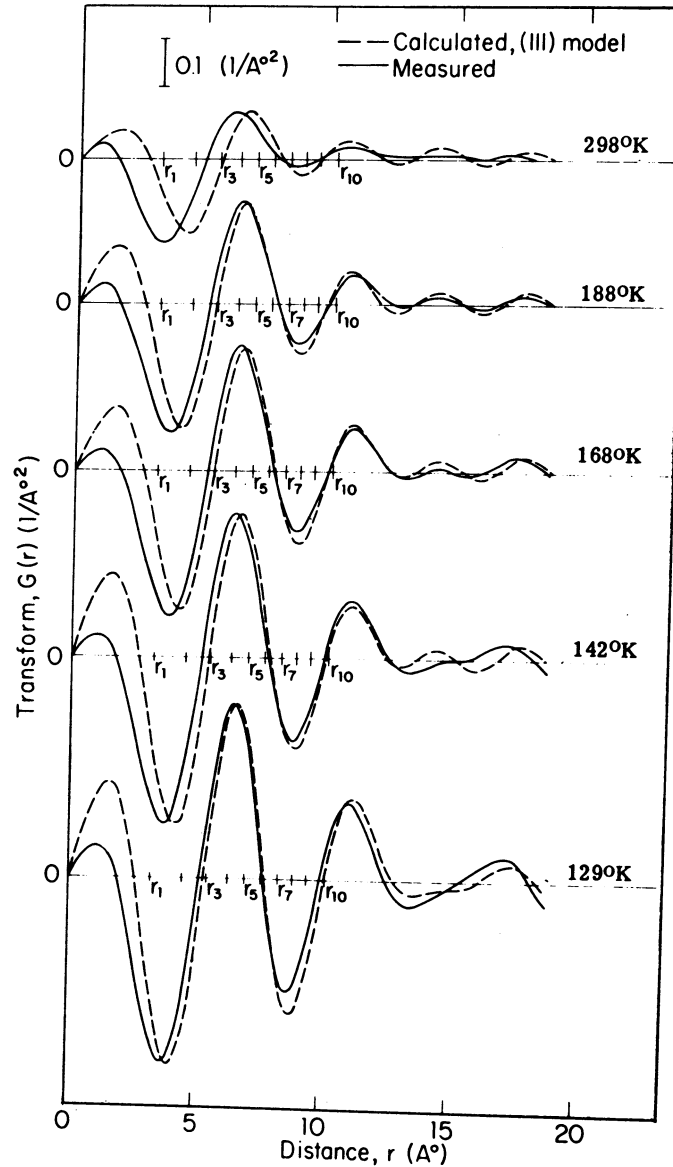


FIGURE 7
Transforms for temperatures above T_N .

The spin correlation γ_i is generally lower and the directional coefficients x_i and y_i are modified. We introduce a directional coefficient, Γ_i , to describe the relative directional order and equation (14) becomes:

$$I(k) = \sum_{i=1}^N c_i |\gamma_i| \Gamma_i \left\{ x_i \frac{\sin kr_i}{kr_i} + y_i \left(\frac{\sin kr_i}{k^3 r_i^3} - \frac{\cos kr_i}{k^2 r_i^2} \right) \right\} \quad (15)$$

It is evident from Table 1 that the values of x_i and y_i for the unmixed shells are the same for the {111} and the {100} models. It can be shown [11] that the x_i and y_i for these shells are independent of the spin

direction in these layered models. The value of Γ_i for the unmixed shells in these layered models is thus unity. The term within the braces $\{ \}$ may be calculated for any model. The coefficients $|\gamma_i|$ indicate the strength of the correlation, and the directional coefficients Γ_i indicate the degree to which the spin directions deviate from the model.

The coefficients $|\gamma_i|\Gamma_i$ were determined by using the intensity function between $k = .25$ and $k = 1.8A^{-1}$ and fitting the transforms calculated for each shell, i , to the experimental transform [12]. The transforms for the $\{111\}$ model are compared in Figure 7. The values of γ_i were determined directly for the unmixed shells (since Γ_i (unmixed) = 1), and these are listed in Table 2. The experimental values of $|\gamma_i|$ (unmixed) are

TABLE 2
Spin Correlation Coefficients in
Disordered MnO

$^{\circ}\text{K}$	γ_2	γ_4	γ_6
129	-0.22	0.16	-0.13
142	-0.21	0.13	-0.09
168	-0.19	0.11	-0.08
188	-0.17	0.09	-0.05
298	-0.12	0.03	-0.01

shown in Figure 8. The alternating signs of the spin correlation coefficients are consistent with the assumption that a layering type of local order exists above the Neel temperature. The spin correlation de-

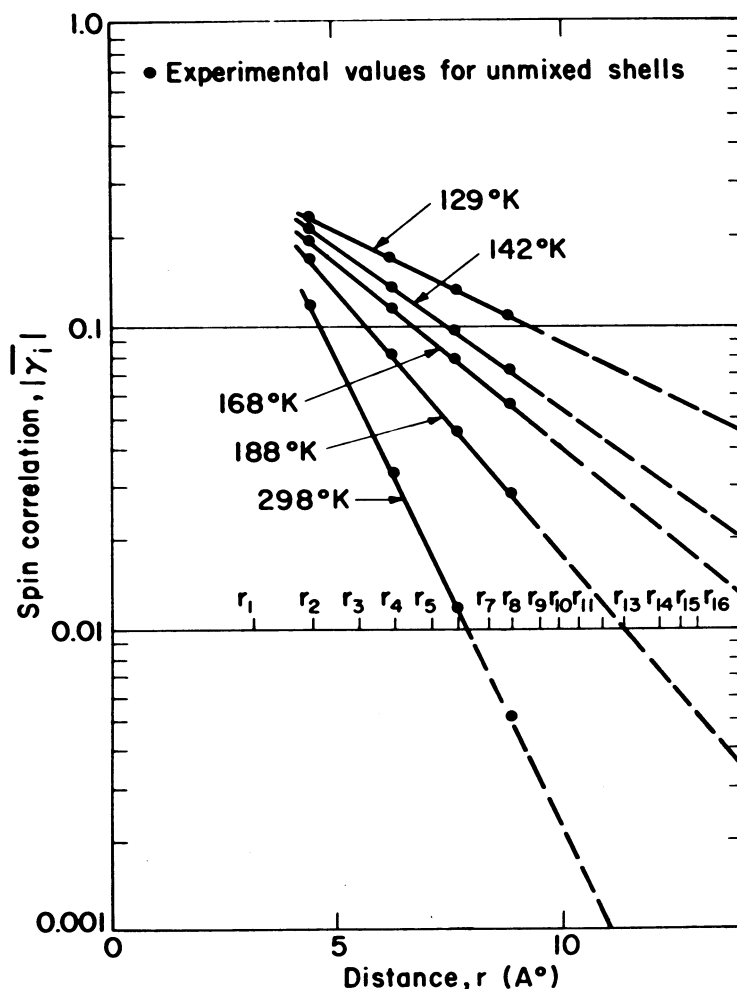


FIGURE 8

Spin correlation, $|\gamma_i|$, as a function of correlation distance.

creases with interionic distance and with increasing temperature. The short range spin order decreases rapidly with distance at elevated temperatures, corresponding to smaller ordered regions.

The coefficients $|\gamma_i|\Gamma_i$ for the mixed shells are listed in Table 3. A careful distinction should be made between γ_i , $\bar{\gamma}_i$ and $|\gamma_i|$. The quantity γ_i is the value of the individual spin correlation coefficient for each

TABLE 3
Spin Correlation Products in Disordered MnO

$^{\circ}\text{K}$	Γ_1	$ \gamma_1 \Gamma_1$	$ \gamma_3 \Gamma_3$	$ \gamma_5 \Gamma_5$
129	0.6	0.17	0.12	0.09
142	0.5	0.16	0.09	0.06
168	0.4	0.11	0.06	0.04
188	0.4	0.10	0.05	0.03
298	0.2	0.04	0.01	0.00

atom in the i^{th} shell; the quantity $|\gamma_i|$ is the absolute magnitude of the individual coefficient. The quantity $\bar{\gamma}_i$ is the average of the coefficients over the entire i shell. For unmixed shells, $\gamma_i = \bar{\gamma}_i$. For mixed shells $\bar{\gamma}_i = 0$ for the layered models, since there are an equal number of parallel and antiparallel spins. However, $|\gamma_i|$ and γ_i are not zero, but values of $|\gamma_i|$ for mixed shells cannot be determined without additional assumptions. The coefficients $|\gamma_i|\Gamma_i$ cannot be separated unless one of the quantities is known. We have estimated values of $|\gamma_i|$ by extrapolation in Figure 8. The corresponding values of Γ_1 are listed in Table 3. These estimates of Γ_1 are quite approximate, but they seem to decrease with temperature. Only the correlation products for the other mixed shells are listed, since any attempts at separation would be very inaccurate.

The relative intensity function, $I(k)$, may be calculated from the derived coefficients and the resultant curve in Figure 9 shows that experimental data are in reasonably close agreement with the $\{111\}$ model. A

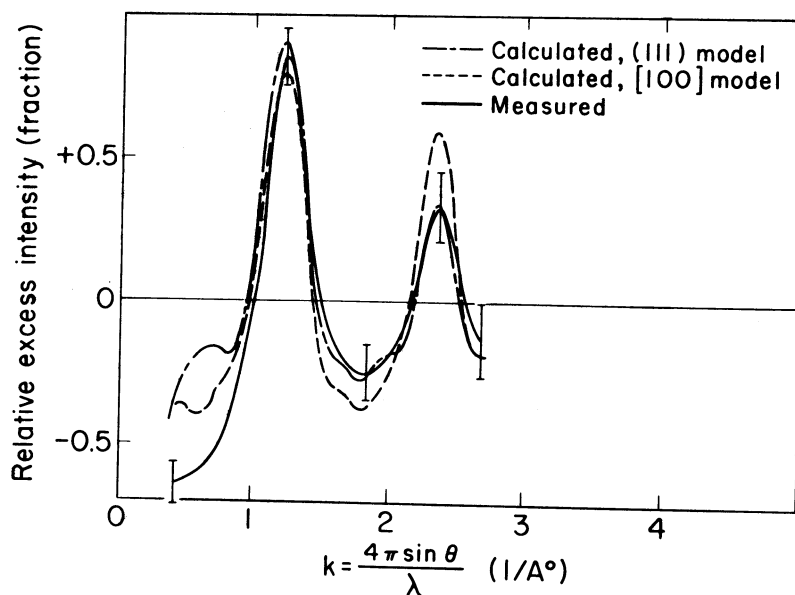


FIGURE 9
Comparison of intensity function for $\{111\}$ and $\{100\}$ models.

calculation for the $\{100\}$ model, with the coefficients chosen to give a good fit for the first diffuse peak, results in a second diffuse peak which is too high. The difference is beyond the estimated accuracy of the data, and we conclude that the spins tend to remain parallel to $\{111\}$ planes at temperatures above the Néel temperature. This model is not unique and it was assumed because it fits the ordered structure quite well.

IV. Discussion

It is evident from Table 2 that the second nearest neighbor spins are antiparallel and the fourth neighbor spins are parallel in the disordered condition. This is consistent with the retention of a layered spin ar-

rangement above the Néel temperature. The data in Table 3 also show that the individual spin correlations, γ_i , do not vanish for the first, third and fifth neighboring shells; however, the average moment for these mixed shells, $\bar{\gamma}_i$, is negligibly small, even above T_N . This result does not depend on our choice of model but is determined by the character of the experimental transforms in Figure 7 which are directly related to the modulations of the magnetic moment in the crystal. For example, it is impossible to account for the transforms, and thus the scattered intensity, with any arrangement in which the nearest neighbor coefficient, $\bar{\gamma}_1$, is not very close to zero. A calculation in which the coefficients B_i are everywhere zero results in values of $\bar{\gamma}_i$ which are not substantially different from those listed in Table 2. There is some evidence, however, for the existence of a small nearest neighbor spin correlation along with the predominant layered structure. A comparison of the transforms in Figure 7 shows that the first negative observed peak is shifted systematically to the left of the calculated peak with increasing temperatures. This may indicate that there is a small net negative correlation coefficient, $\bar{\gamma}_1$, for the first shell. At 298°K, where the shift is greatest, a better fit to the transform is obtained with $\bar{\gamma}_1 = -0.02$, $\bar{\gamma}_2 = -0.12$, and with the remaining coefficients unchanged. It is thus possible that there is a small amount of nearest neighbor short range spin order in MnO above the Néel temperature, but even at 298°K the predominant spin arrangement is a layered antiferromagnetic structure similar to that of the ordered structure.

The superexchange interaction energy was estimated from the temperature variation of the second neighbor coefficients. We define p_u as the probability that a given spin is antiparallel to a spin at the origin. The quantity γ then becomes:

$$\gamma = \frac{(1 - 2p_u)S^2}{S(S + 1)} \quad (16)$$

The interaction energy then becomes [13],

$$\frac{p_u}{1 - p_u} = \exp(-V_2/kT) \quad (17)$$

where V_2 is the interaction energy for the second nearest neighbors. Using the data in Table 2, a value of $V_2 = -4.9 \times 10^{-3}$ eV is obtained. This corresponds to a value of $J_2/k = -4.65^\circ$ for the exchange integral, and this is in the same range as the values of J_2 summarized by Smart [14]. This calculation is meaningful if the superexchange mechanism is dominant and the second neighbor interaction energy is not affected by the first neighbor interaction. It is thus possible to have finite values of J_1 for individual nearest neighbor

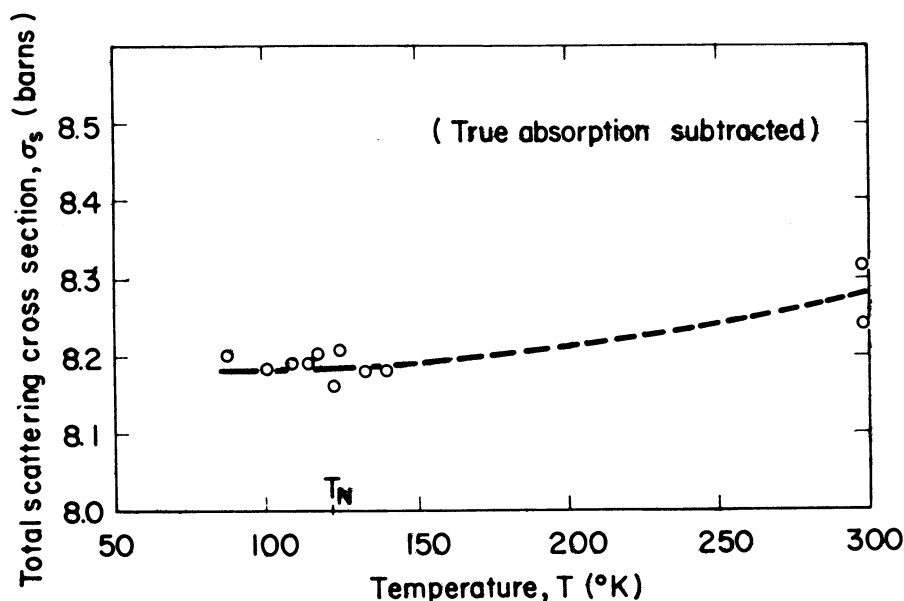


FIGURE 10
MnO total scattering cross section.

spins, but since the directional effect results in a net value of $\bar{\gamma}_1 = 0$, we are unable to make any estimate of J_1 from these data.

From Figures 3 and 4 it is seen that the first maximum in the diffuse scattering increases with decreasing temperature until a maximum is reached at the Néel temperature. There is a sharp decrease in the diffuse scattering just below T_N , and the diffuse peak continues to decrease gradually as the temperature is lowered. This behavior has been described as a critical scattering [8]. Critical scattering, as introduced by Van Hove [15], is characterized by an increase in the total scattering cross section. We have measured the total scattering cross section of MnO by transmission experiments (Figure 10). The total cross section of MnO was determined from the attenuation of a small beam passing through the sample. The total scattering cross section was then found by subtracting the true absorption from the total cross section. We have not detected any significant increase in the cross section in the vicinity of the Néel temperature. It is concluded that the apparent decrease in the diffuse hump at subcritical temperature results from the onset of long range spin order which reduces the number of spins contributing to the diffuse scattering. The co-existence of the diffuse peak with the superlattice reflection (Figure 1) suggests that the same type of short range spin correlations observed above T_N persist below the Néel Temperature.

Acknowledgements

The authors would like to acknowledge the support of the National Science Foundation and the assistance of the Hebrew Technical Institute to one of us (IAB). We would also like to acknowledge the many valuable discussions with Professor C. G. Shull and the help received from Professor Roy Kaplow and Mr. Stephen L. Strong. The assistance of the MIT Computation Center is also gratefully acknowledged.

References

1. H. BIZETTE, C. F. SQUIRE and B. TSAI, *C. R. Acad. Sci., Paris* **207**, 449 (1938).
2. C. G. SHULL, W. A. STRAUSSER and E. O. WOLLAN, *Phys. Rev.* **83**, 333 (1951).
3. W. L. ROTH, *Phys. Rev.* **110**, 1333 (1958).
4. A. L. LOEB and J. B. GOODENOUGH, *Conference on Magnetism and Magnetic Materials*, Boston, Mass., October 16–18, 1956 (unpublished).
5. A. W. McREYNOLDS and T. RISTE, *J. Phys. Rad.* **20**, 179 (1959).
6. G. E. BACON, *Neutron Diffraction*, Oxford, London (1962).
7. N. KURIYAMA and F. HOSOYA, *J. Phys. Soc. Japan* **17**, 1022–9 (1962).
8. P. G. DE GENNES, *Magnetism* (Edited by O. T. RADO and H. SUHL) Vol. III. Academic Press, New York (1963).
9. J. M. COWLEY, *Phys. Rev.* **77**, 699 (1950).
10. B. E. WARREN, *Lectures on X-ray diffraction*, M.I.T.
11. I. A. BLECH, Sc.D. Thesis, M.I.T., 1964.
12. R. KAPLOW, *ASM Technical Paper* 15.1 October 1963.
13. E. A. GUGGENHEIM, *Mixtures*. Clarendon Press, Oxford (1952).
14. J. S. SMART, *Magnetism* (Edited by O. T. RADO and H. SUHL) Vol. III. Academic Press, New York (1963).
15. L. VAN HOVE, *Phys. Rev.* **95**, 262 (1954).